Chaos
An Interdisciplinary Journal of Nonlinear Science

Collective excitability in highly diluted random networks of oscillators

Cite as: Chaos **32**, 103108 (2022); https://doi.org/10.1063/5.0102880
Submitted: 13 June 2022 • Accepted: 12 September 2022 • Published Online: 14 October 2022

Gabriele Paolini, Marzena Ciszak, Francesco Marino, et al.

Collective excitability in highly diluted random networks of oscillators

Cite as: Chaos **32**, 103108 (2022); doi: 10.1063/5.0102880
Submitted: 13 June 2022 · Accepted: 12 September 2022 ·
Published Online: 14 October 2022

Gabriele Paolini,[1] Marzena Ciszak,[2,a)] Francesco Marino,[2,3,b)] Simona Olmi,[3,4,c)] and Alessandro Torcini[1,3,4,d)]

AFFILIATIONS

[1]Laboratoire de Physique Théorique et Modélisation, UMR 8089, CY Cergy Paris Université, CNRS, 95302 Cergy-Pontoise, France
[2]CNR—Consiglio Nazionale delle Ricerche—Istituto Nazionale di Ottica, via Sansone 1, 50019 Sesto Fiorentino, Italy
[3]INFN, Sezione di Firenze, via Sansone 1, 50019 Sesto Fiorentino, Italy
[4]CNR—Consiglio Nazionale delle Ricerche—Istituto dei Sistemi Complessi, via Madonna del Piano 10, 50019 Sesto Fiorentino, Italy

Note: This paper is part of the Focus Issue on Disruption of Networks and System Dynamics.
[a)]**Electronic mail:** marzena.ciszak@ino.cnr.it
[b)]**Electronic mail:** francesco.marino@ino.cnr.it
[c)]**Electronic mail:** simona.olmi@cnr.it
[d)]**Author to whom correspondence should be addressed:** alessandro.torcini@cyu.fr

ABSTRACT

We report on collective excitable events in a highly diluted random network of non-excitable nodes. Excitability arises thanks to a self-sustained local adaptation mechanism that drives the system on a slow timescale across a hysteretic phase transition involving states with different degrees of synchronization. These phenomena have been investigated for the Kuramoto model with bimodal distribution of the natural frequencies and for the Kuramoto model with inertia and a unimodal frequency distribution. We consider global and partial stimulation protocols and characterize the system response for different levels of dilution. We compare the results with those obtained in the fully coupled case showing that such collective phenomena are remarkably robust against network diluteness.

Collective excitable phenomena in a system of coupled elements may arise either when the single nodes display excitable dynamics or not. The latter case, more surprisingly, is possible when the entire ensemble of nodes is subject to a global feedback depending self-consistently on the level of synchronization of the network. In this case, a global excitable response to an external stimulus can be observed, which corresponds, at the microscopic level, to a transient partial synchronization of the nodes. Mathematically, this is related to hidden geometric structures that organize the mean field trajectories in the phase space. These events have been observed in two paradigmatic classes of globally coupled oscillators, namely, the Kuramoto model with and without inertia. In this paper, we analyze the robustness of the collective excitability in highly diluted random networks by gradually decreasing the percentage of coupled nodes. We consider global and partial stimulation protocols, and we characterize the response with respect to that achievable in the corresponding fully coupled network. Our findings demonstrate remarkable robustness of the collective excitability, which we expect to inspire new research in the study of emergent phenomena in networks of interacting elements at the mesoscopic scale.

I. INTRODUCTION

Excitable systems appear in many scientific fields; in particular, they have been studied in the context of neuroscience as simplified neural models[1] as well as in cardiac dynamics for pulse propagation.[2] Several low-dimensional models have been introduced to reproduce the excitable properties of the cells. All these models are characterized by few common features: They all present a linearly stable fixed point that, once stimulated with a sufficiently large perturbation, displays a large excursion in the phase space corresponding to the emission of a pulse of well-defined amplitude and duration. These low-dimensional slow–fast systems show a very rich dynamical repertoire, characterized by regular and chaotic spiking and

bursting behaviors, and joined to extremely complex bifurcation structures.[3–8]

Collective excitable responses and bursting activities have been previously reported in networks of excitable nodes for globally coupled populations[9,10] as well as for spatially extended systems, where they appear in the form of excitable waves[11] and as transient synchronization states.[12,13]

A few studies[14–17] have recently shown that collective excitable dynamics can emerge also in networks of non-excitable units, such as oscillators, in the presence of a global linear feedback. In particular, in Ref. 16, the effect of a global linear feedback on the dynamics of the Kuramoto model with and without inertia has been investigated. Thanks to the feedback, the system originally characterized by hysteretic first-order transitions[18–22] reveals collective dynamical features typical of excitable models, despite a nonexcitable single-node dynamics. The origin of these behaviors is related to the competition of the fast synchronization/desynchronization phenomena triggered by the slow adaptation.

All the previous studies[14–17] have been devoted to globally coupled networks, where the coupling among the oscillators was dynamically adjusted based on a single feedback loop dependent on the level of synchronization in the whole system. The global nature of the coupling has allowed us to derive an exact low-dimensional mean field formulation for the Kuramoto model with bimodal frequency distributions by applying the Ott–Antonsen ansatz in this context,[23] thus making possible to explain the collective excitability of the model in terms of the stability properties of a slow invariant one dimensional manifold and to demonstrate a strict analogy with the dynamical behavior of the Hindmarsh–Rose model for a single neuron.[16,17]

Despite the fact that globally coupled systems are amenable of extremely effective analytical treatments, more realistic networks, as the brain circuits, are characterized by sparse random connections. The randomness in the connections can change drastically the nature of the synchronization transition[24,25] and have a strong influence on the collective behaviors.[26] Therefore, it is of extreme interest to study if the phenomenon of collective excitability observed in globally coupled systems is robust to random pruning of the connections and how the dynamics is modified due to the sparseness of the connections. To our knowledge, the case of nonglobal interactions has been addressed only in one study reported in Ref. 15. In such a case, the authors considered a random network with power-law distributed degrees, where each oscillator was subject to a local feedback involving its random neighbors. A detailed analysis of the parameter space revealed the emergence of regimes similar to those observed in the globally coupled case (bistable, synchronized, excitable, oscillatory, and incoherent states). However, the considered network was not particularly diluted since each oscillator was connected on average to 18% of the whole oscillators, and, in general, the number of connections is never less than 10% of the oscillators.

In the present paper, starting from Ref. 16, we investigate how a highly diluted random network of non-excitable nodes can become collectively excitable thanks to a self-sustained local adaptation mechanism. In particular, we have studied in detail the excitability response of the network to perturbations by considering global and partial stimulation protocols for different levels of dilution. This analysis has been performed for the Kuramoto model with a bimodal distribution of the natural frequencies and for the Kuramoto model with inertia with a unimodal frequency distribution. This paper is structured as follows. The investigated models and the indicators employed to characterize the excitability features of the system as well as the stimulation protocols are described in Sec. II. The results of the numerical investigations are reported in Sec. III, for the bimodal Kuramoto model (BKM) and the Kuramoto model with inertia (KMI), by considering the response of the network to global stimulations and to stimulation affecting only a fraction of the oscillators. Finally, in Sec. IV, a brief discussion on the results is reported.

II. MODEL AND INDICATORS

A. Network model

We consider a heterogeneous network of N oscillators characterized by their phases $\{\theta_n(t)\}$ and angular velocities $\{\dot{\theta}_n(t)\}$, where each oscillator is randomly coupled to M neighbors via an adaptive coupling that is dependent on the level of synchronization among the neighbors themselves. The evolution equations for the phases are given by

$$m\ddot{\theta}_n + \dot{\theta}_n(t) = \omega_n + \frac{S_n(t)}{M}\sum_{j=1}^{N}\mathcal{C}_{nj}\sin(\theta_j - \theta_n), \tag{1}$$

$$\dot{S}_n(t) = \varepsilon[-S_n + K - \alpha Q_n(t)], \tag{2}$$

where ω_n is the natural frequency of the nth oscillator, m its mass, and $S_n(t)$ an adaptive coupling controlled via a linear feedback by the modulus $Q_n(t)$ of the local Kuramoto order parameter, which is defined as

$$Q_n(t) = \frac{1}{M}\left|\sum_{j=1}^{N}\mathcal{C}_{nj}\, e^{i\theta_j(t)}\right|. \tag{3}$$

This quantity characterizes the level of synchronization among the M neighbors of the nth oscillator and its value ranges from $Q_n = 1$, if they are fully synchronized, to $Q_n \simeq \mathcal{O}\left(1/\sqrt{M}\right)$ in case they are completely asynchronous. The gain of the feedback loop is controlled by the real positive parameter α, its bandwidth by ε, which usually sets to $\varepsilon = 0.01$, while $K > 0$ represents the asymptotic coupling to which S_n would relax in the absence of any synchronization among the neighbors. The stationary value of the adaptive coupling ranges from $S_{FS} = K - \alpha$, for a fully synchronized case, to $S_{AS} \simeq K - d\frac{\alpha}{\sqrt{M}}$ for an asynchronous state, where d is some positive constant $\mathcal{O}(1)$. Therefore, when the system is fully synchronized, the adaptive coupling will relax toward S_{FS}, a coupling value corresponding to asynchronous dynamics in the original system without adaptation, while, when it is desynchronized, it will relax toward S_{AS} that, for $M >> 1$, is definitely larger than S_{FS}, and it corresponds to a bistable regime in the original setup.[16] However, for a small M degree, the latter is no more verified. In particular, it is evident that S_{AS} will change sign at $M_c \simeq \left(\frac{\alpha}{K}\right)^2$, thus indicating a passage from a repulsive ($M < M_c$) to an attractive ($M > M_c$) adaptive coupling.

The matrix $\{\mathcal{C}_{nj}\}$ is an adjacency matrix, where $\mathcal{C}_{nj} = 1$ ($\mathcal{C}_{nj} = 0$) if an undirected link exists (non-exists) among oscillators n and j. Similarly, to the Erdös–Rényi random graph,[27] the adjacency matrix $\{\mathcal{C}_{nj}\}$ is constructed by connecting labeled nodes randomly, where each link is included in the graph independently from every other link. However, at variance with the Erdös–Rényi graph, here, the degree of each oscillator n is fixed exactly to $M = \sum_{j=1}^{N} \mathcal{C}_{nj} = \sum_{j=1}^{N} \mathcal{C}_{jn}$.

Since collective excitable behaviors emerge in (1) and (2) for a fully coupled network (where $M \equiv N$) whenever the coexistence of two stable regimes characterized by different levels of synchronization exists,[15,16] we will focus on systems exhibiting hysteretic synchronization transitions. Therefore, to show the generality of our results, we considered two quite different cases within this class of systems: namely, the KMI (1) with a unimodal distribution of the frequencies and the Kuramoto model [$m = 0$ in (1)] with a bimodal distribution of the natural frequencies (BKM). In order to compare with the results reported in Ref. 16 for the fully coupled case, we will consider for the KMI $m = 2$ and Gaussian distributed frequencies with zero mean and a unitary standard deviation and for the BKM bimodal Lorentzian distributed frequencies. The Lorentzian distributed frequencies are fixed deterministically as follows:

$$\omega_j = -\omega_0 + \Delta \tan\left[\frac{\pi}{2}\xi_j\right], \quad \xi_j = \frac{2j - \frac{N}{2} - 1}{\frac{N}{2} + 1}, \quad j = 1, \ldots, \frac{N}{2},$$
$$\omega_j = \omega_0 + \Delta \tan\left[\frac{\pi}{2}\xi_j\right], \quad \xi_j = \frac{2j - \frac{3N}{2} - 1}{\frac{N}{2} + 1}, \quad j = \frac{N}{2} + 1, \ldots, N, \tag{4}$$

where $\pm w_0$ is the position of the two peaks, each characterized by the same half-width half-maximum Δ. The deterministic choice in (4) allows us to reduce finite size effects due to the imbalance between positive and negative frequencies that can have dramatic effects for Lorentzian distributions when randomly sampled.[28] The parameters entering in (4) have been fixed to $w_0 = 1.8$ and $\Delta = 1.4$.

All the numerical simulations have been performed by employing a fourth order Runge–Kutta integration scheme with a time step $\delta t = 0.1$; the system has been usually investigated for a time duration $t_D = 800$.

B. Coherence measure

The microscopic evolution of the oscillators has been visualized via a sort of a *raster plot*, commonly used in the context of neural dynamics. To be more specific, for each oscillator, we depict a dot in correspondence with the time instant the oscillator phase crosses a fixed threshold; in our case, the threshold has been fixed to $\theta_{th} = 0$.

In order to characterize the collective dynamics of the system, we will rely on the global Kuramoto order parameter[29]

$$R(t) = \frac{1}{N}\left|\sum_{j=1}^{N} e^{i\theta_j(t)}\right|. \tag{5}$$

In the absence of coupling adaptation, one typically observes an asynchronous (partially synchronous) regime characterized by $R \simeq \mathcal{O}(1/\sqrt{N})$ (finite R) for small (large) coupling strengths.[30]

C. Stimulation protocols

In this work, since we want to analyze the excitable properties of the system, we are interested in observing the response of the system to perturbations. In particular, we will perturb instantaneously the adaptive coupling term $S_n(t)$ of the oscillator n by increasing its value of a constant amount A at time t: i.e., $S_n(t^+) = S_n(t^-) + A$. If all oscillators are perturbed at the same time, this corresponds to perform a *global stimulation* of the system; instead, if only a percentage P of oscillators is perturbed, this will be termed *partial stimulation*.

In particular, we usually stimulate the oscillators irrespectively of their natural frequencies for the KMI, while, for the BKM, we usually stimulate by starting from the central node with index $N/2$ and then moving symmetrically toward nodes with larger and smaller indices (protocol zero). For the BKM besides this protocol, we also consider two other different stimulation protocols defined as follows: (protocol one) the oscillators are stimulated by considering first the ones with natural frequencies $\omega_i \simeq |w_0|$ in proximity of the two peaks of the frequency distribution function and then, symmetrically, the oscillators with larger values of $|\omega_i - \omega_0|$ and $|\omega_i + \omega_0|$; (protocol two) is the same protocol as protocol one, but referred only to one peak, namely, the one located at $-\omega_0$; therefore, the oscillators are stimulated asymmetrically starting from the ones in proximity of only one of the two peaks of the distribution.

The excitable response of the system to the stimulations has been characterized in terms of the global Kuramoto order parameter $R(t)$; a collective burst is identified whenever $R(t)$ overcomes a threshold value R_{th} within a given time window W_{test} after the perturbation deliverance. Furthermore, we measured the maximum value R_m at the burst peak as well as the time T_m needed to reach such a peak after the stimulation. For the BKM, we fixed $R_{th} = 0.4$ to distinguish bursting events from the underlying collective oscillations of amplitude $\simeq 0.2 - 0.3$, while for the KMI, we set $R_{th} = 0.2$ since the stationary dynamics, in this case, is asynchronous apart from finite size fluctuations. In both cases, $W_{test} = 200$.

III. RESULTS

In the following, we will consider parameter values for which the fully coupled adaptive networks ($M = N$) display collective excitable properties for BKM and KMI, as reported in Ref. 16, and we will examine the response of the randomly diluted systems ($M << N$) to global and partial stimulations by varying M as well as the percentage P of stimulated oscillators.

In particular, for the BKM, by following Ref. 16, we analyze a situation where the fully coupled system displays collective periodic oscillations, characterized by the alternation of partially synchronized phases with abrupt desynchronization events. These collective solutions are usually termed *standing waves*[19] in the context of networks of coupled oscillators and *spikes* for the analogy with the Hindmarsh–Rose model developed in Ref. 16. This regime persists also for diluted systems, as shown in Fig. 1(a) (black trace) for $K = 6.9$, $\alpha = 5$, $M = 1000$, and $N = 5000$. For what concerns the collective excitable properties of the KMI, we will consider a purely asynchronous phase, where $R(t)$ shows irregular fluctuations

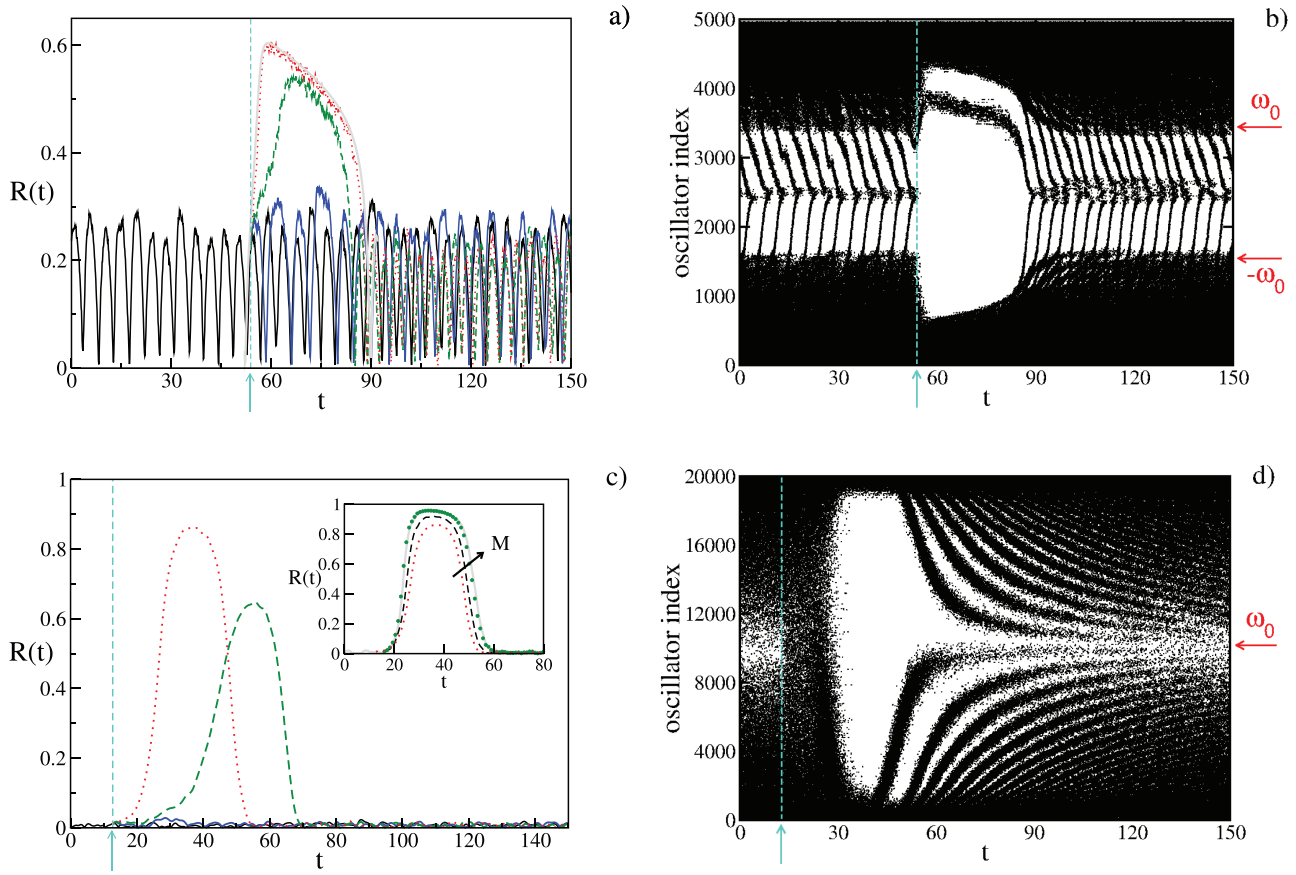

FIG. 1. BKM: (a) Global order parameter R vs time for a network with random connectivity (degree $M = 1000$) in the spiking regime (black solid line). The system responses to global perturbations for different amplitudes A are also displayed: a subthreshold response for $A = 0.150$ (blue solid line) and two excitable responses for $A = 0.200$ (green dashed line) and for $A = 0.375$ (red dotted line). The system response of the fully coupled network for $A = 0.375$ is shown in gray. (b) Raster plot for the diluted network obtained as a response to a perturbation of amplitude $A = 0.375$; here, the oscillators are sorted by frequency in an ascending order. Other parameters: $\varepsilon = 0.01, \Delta = 1.4, \omega_0 = 1.8, \alpha = 5, K = 6.9$, and network size $N = 5000$. KMI: (c) Global order parameter R vs time for a network with random connectivity ($M = 50$) in the asynchronous regime (black solid line). In the same panel, the system responses to global perturbations of different amplitudes A are also displayed: a subthreshold response for $A = 4.2$ (blue solid line) and two excitable responses for $A = 5$ (green dashed line) and for $A = 6$ (red dotted trace). In the inset, the response to a perturbation of amplitude $A = 6$ is displayed for different values of the degrees: $M = 50$ (red dotted line), $M = 100$ (black dashed line), $M = 500$ (green dots), and $M = N$ (gray shaded curve). (d) Raster plot for the diluted network with $M = 50$ and for a stimulation of amplitude $A = 6$; also, in this case, the oscillators are sorted by frequency in an ascending order. Other parameters: $\varepsilon = 0.01, \alpha = 30, K = 4.5, m = 2, \omega_0 = 0$ and network size $N = 20\,000$. The cyan arrows and the cyan dashed lines denote the time of the instantaneous stimulation.

of amplitude $\mathcal{O}(1/\sqrt{N})$; this occurs for $\alpha = 30$ and $K = 4.5$, as shown in Fig. 1(c) (black solid line) for $M = 50$ and $N = 20\,000$.

A. Global stimulation

1. Bimodal Kuramoto model

Let us first consider the BKM in the standing wave regime, characterized by periodic sequences of collective spike events, where the corresponding time evolution of $R(t)$ is reported as a solid line in Fig. 1(a). In this situation, the system displays collective excitability when globally stimulated despite that the oscillators are randomly connected with high dilution $M \ll N$. Indeed, small contemporary perturbations of all the feedback variables $S_n(t)$ elicit rapidly decaying responses in $R(t)$ [blue trace in Fig. 1(a)], while sufficiently large stimuli induce a synchronized activity in a considerable part of the network, characterized by an evolution of $R(t)$ corresponding to a large amplitude oscillation with a well-defined shape, amplitude, and duration (green trace). This collective event can be seen as an oscillation connecting a tonic spiking regime to a silent (resting) state, and it is analogous to the so-called *burst*, typical of the dynamics of several neurons.[31] Furthermore, a larger perturbation gives rise to a bigger burst (red dotted line) that involves more synchronized oscillators and approaches an asymptotic shape,

essentially corresponding to that observed in the fully coupled network for the same perturbation amplitude A_0 (gray curve). This is despite the system being diluted with a clustering coefficient $c = M/N = 20\%$.[32]

The mechanism leading to the emergence of a burst can be better understood by examining the corresponding raster plot reported in Fig. 1(b). In the period before the moment of the stimulation (denoted by a cyan arrow and a dashed cyan line), one observes a regime characterized by standing waves propagating from oscillators with natural frequencies $\pm\omega_0$ toward the oscillators with zero frequency. Immediately after the stimulation, a wider group of oscillators with natural frequencies in the interval $[-\omega_0 - \Delta; \omega_0 + \Delta]$ phase lock, while the remaining oscillators with larger natural frequencies (in absolute value) are not entrained to the big synchronized cluster. This is the origin of the burst, as measured by the order parameter $R(t)$, and it corresponds to the silent state reached during a neuronal burst. The number of the synchronized oscillators slowly decreases in time, but it remains essentially unmodified for a duration $t_d \simeq 30$, soon after the burst disappears and the standing waves re-emerge in the network.

It is important to remark that, for $M < 50$, spikes are hardly discernible from the fluctuations of R due to the network sparsity, thus setting the minimal degree that can be analyzed, for the BKM, to $M = 50$, corresponding to a clustering coefficient $c = M/N = 1\%$.

2. Kuramoto model with inertia

In the case of the KMI, the unperturbed state is asynchronous, in contrast to the BKM, as evident from the evolution of $R(t)$ reported as a solid black line in Fig. 1(c). However, also in this case, the system displays collective excitability when globally stimulated, even in the very diluted case: namely, we considered $M = 50$, corresponding to a clustering coefficient $c = 0.25\%$ for $N = 20\,000$. Indeed, small perturbations of amplitude $A = 4.2$ elicit no collective response (blue solid line), while larger perturbations ignite bursts, as shown in Fig. 1(c) for $A = 5$ (green dashed line) and $A = 6$ (red dotted line). This demonstrates the existence of a threshold value A_0, which should be overcome to observe an excitable response when globally perturbing the system. Furthermore, as shown in the inset of Fig. 1(c), the shape of the burst approaches that obtained in the globally coupled case by increasing M; already for $M = 500$ (green dots), the asymptotic profile corresponding to $M = N$ is essentially recovered.

On the other hand, the collective response of the system to a stimulation is quite different for the KMI with respect to the BKM, as shown in Fig. 1(d). In particular, there is a transient period of duration $t_T \simeq 15$ before the onset of the burst that was definitely shorter in the BKM case. During the burst, at variance with the BKM almost all oscillators are phase locked. At its disappearance, we observe that, due to inertia, the oscillators with natural frequencies in proximity of the peak of the distribution located at $\omega_0 = 0$ relax faster to the asynchronous regime than those far away in the distribution itself characterized by higher natural frequencies $|\omega_i|$.

3. Comparison of BKM and KMI analysis

As a first analysis, we investigate the value of the minimal perturbation amplitude A_0 needed to ignite a collective burst as a function of the network degree M. The results of the analysis are reported in Fig. 2 for both the BKM and KMI. While in the BKM, we cannot consider $M < 50$, otherwise, the spiking activity will be

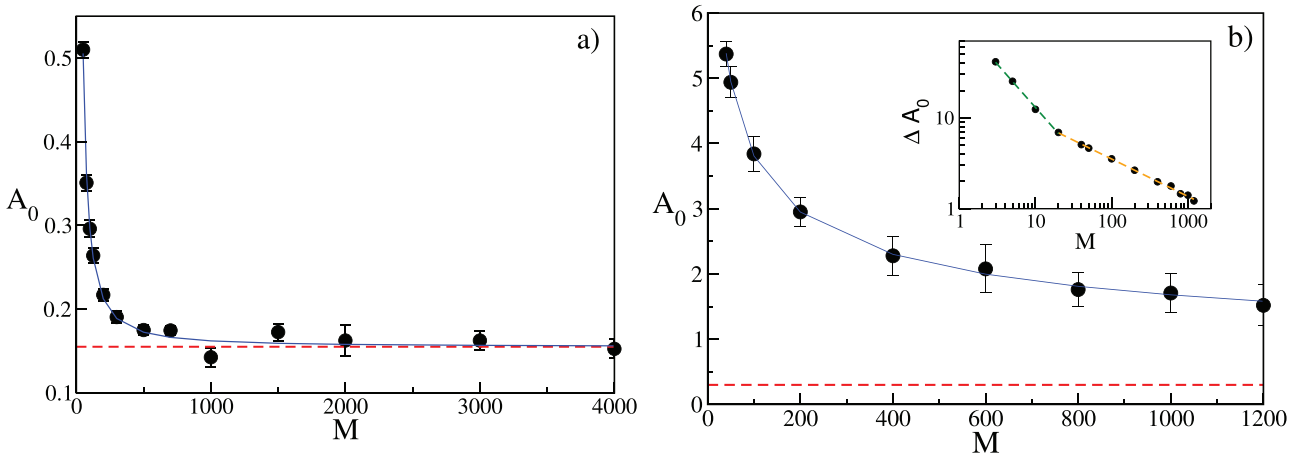

FIG. 2. Minimal perturbation amplitude A_0 required to observe a collective burst as a function of the degree M: (a) BKM and (b) KMI. The red dashed lines represent the values $A_0^{(FC)}$ of the minimal perturbation amplitude for the corresponding fully coupled networks. The blue solid line denotes a nonlinear fitting to the data $A_0 \simeq A_0^{(FC)} + a/M^\beta$ $A_0^{(FC)} \simeq 0.155$ ($\simeq$0.299), $a \simeq 57.86$ ($\simeq$22.66) and $\beta \simeq 1.30$ ($\simeq$0.40) for the BKM in (a) [KMI in (b)]. In the inset of panel (b), the green (orange) dashed lines refer to a power-law fit $\Delta A = A_0 - A_0^{(FC)} \simeq a/M^\beta$ to the data for the interval $3 \leq M \leq 20$ ($20 \leq M \leq 1200$) with an exponent $\beta \simeq 0.95$ ($\beta \simeq 0.41$). For the BKM for $M < 1000$, we averaged A_0 over 50–100 network realizations, while for greater values of M, we averaged over 10 realizations due to higher computational time; for the KMI, we always averaged over 20 network realizations. In both panels, the error bars correspond to the standard deviation of the mean. Parameters as in Fig. 1, apart from $K = 4.0$ for the KMI.

no more discernible from the background noise; for the KMI, the dynamics remains asynchronous even for vanishingly small M. In the latter case, it is possible to observe a collective response up to $M = 3$ with a sufficiently large perturbation A_0 [as shown in the inset of Fig. 2(b)]. However, no response was observable for $M = 1$ and 2 even for extremely large A_0. This is probably due to the existence (or not) of a giant component in our random network. As a matter of fact, for the random network we are analyzing, where the degree is always exactly M, the giant component emerges via a phase transition occurring at $M = 2$, while for an Erdös–Renyi network, the giant component appears whenever $M \geq 1$.[32,33]

On one hand, for the BKM, the minimal amplitude A_0 approaches the fully coupled value $A_0^{(FC)} \simeq 0.155$ with a power-law decay as $A_0 \simeq A_0^{(FC)} + a/M^{\beta}$, with an exponent $\beta \simeq 1.30$. The fitting to the data is reasonably good and reported as a blue solid line in Fig. 2(a). On the other hand, for the KMI, the approach to the fully coupled case seems definitely more complex. In this case, A_0 decreases quite rapidly at small $M \leq 20$, decaying as $\propto 1/M$, while at larger M, we still observe a power-law decay of $A_0 \propto M^{-\beta}$, but with a definitely smaller exponent $\beta \simeq 0.4$. This crossover from a fast to slower decay of A_0 with the degree is clearly visible in the inset of Fig. 2(b), where $\Delta A_0 = A_0 - A_0^{(FC)}$ is reported for $3 \leq M \leq 1200$.

The fact that the exponent β is definitely larger for the BKM with respect to the KMI case, when approaching the fully coupled case, can be probably related to the fact that it is easier to elicit a collective burst in a system presenting already a partial synchronization associated with the standing waves (spiking activity) than in a system finding itself in asynchronous dynamics.

Furthermore, we characterize the emergence of the burst in terms of two indicators associated with the global order parameter $R(t)$, as shown in the inset of Fig. 3(a): the value of the maximum R_m reached by the order parameter, once performed the stimulation, and the time T_m needed to reach such a maximum after the stimulation. As a first analysis, we consider diluted systems with different degrees M, and we globally stimulate the system with perturbations of amplitude A sufficiently large to lead the network with the smallest considered M to a collective burst. In particular, for the BKM (KMI), the minimal considered degree is $M = 100$ ($M = 50$) and $A = 0.4$ ($A = 6.0$). For each fixed M, we measured the average values of R_m and T_m, obtained by considering 100 different realizations of the random network. The results are reported in Figs. 3(a) and 3(b) for the BKM and in Figs. 3(c) and 3(d) for the KMI.

In both cases, we observe that, for increasing M, R_m approaches the corresponding value obtained in the fully coupled case $R_m^{(FC)}$ for the same stimulation amplitude A. The fully coupled valued is approached with a scaling law consistent with $R_m^{(FC)} - a/M^{\beta}$, where $\beta \simeq 1.0 - 1.3$. Analogously, by increasing M, the time needed to reach the maximum of the burst decreases toward the fully coupled value $T_m^{(FC)}$, with a power-law decay consistent with $T_m^{(FC)} + b/M^{\beta}$, where $\beta \simeq 1.0 - 1.4$. The disorder in the distribution of the links, responsible for the intrinsic fluctuations present in the dynamics, makes it extremely hard (numerically) to validate more rigorously the reported nonlinear fitting. However, these results suggest that the finite size corrections for the measured quantities, due to the dilution, should vanish as $\propto M^{-\beta}$ with $\beta \simeq 1.0 - 1.4$ by approaching the fully coupled limit. This prediction should be valid at least at the leading order.

IV. PARTIAL STIMULATION

In this section, we extend the analysis previously performed to take into account the response of the system to partial stimulations. In particular, we investigate the response of the system to perturbations involving different percentages P of the oscillators for different levels of network dilution (measured by the degree M) and for different amplitude stimulations A.

A. Bimodal Kuramoto model

Let us first consider the BKM; in this case, we fix the degree to $M = 200$, and we measure the percentage of bursts elicited by the stimulation for different percentages P of the stimulated oscillators and a certain stimulation amplitude A. In particular, the numerical analysis is performed by considering 1000 different realizations of the network. The corresponding results are reported in Fig. 4(a). As a first insight, we estimated the percentage of bursts emitted in the absence of any stimulation by varying P. The bursts spontaneously emitted correspond to 0.9% of the considered realizations [dashed horizontal line in Fig. 4(a)]. Therefore, below this percentage, the system response will be considered not reliable since we cannot distinguish between spontaneous emission and response to the stimulation. As shown in Fig. 4(a), for any considered value of $0.2 \leq A \leq 0.7$, the number of elicited bursts is below this threshold whenever the number of stimulated oscillators is below 10% of the nodes of the network, corresponding, in this specific case, to 500 oscillators.

From Fig. 4(a), we observe that the number of elicited bursts increases with the percentage P of the stimulated oscillators for any considered amplitude A. However, for $A = 0.2$, even by stimulating all the oscillators, we obtain bursts only in 40% of the realizations. Indeed, this is related to the fact that $A = 0.2$ is slightly below the minimal stimulation amplitude needed to observe a burst for $M = 200$, which corresponds to $A_0 = 0.217 \pm 0.007$.

For larger amplitudes $A > 0.2$, it is possible to observe a burst for each delivered stimulation (corresponding to 100 % of elicited bursts), whenever P is larger than a critical value $P_f = P_f(A)$, which decreases quadratically with A ($P_f(A) \propto A^{-2}$) for $A \geq 0.5$.

In Figs. 4(b) and 4(c), we report the values of R_m and T_m averaged over all the observed bursts for the same amplitudes and percentages of stimulated oscillators analyzed in panel (a). As a general remark, we observe that R_m (T_m) grows (decreases) monotonically with the percentage of the stimulated oscillators only when this value is beyond 30%. As we will see in the following, this is due to finite size effects. Furthermore, for sufficiently large amplitudes ($A \geq 0.4$), the maximal value of the burst tends toward the one measured in the fully coupled network $R_m^{(FC)}$ for the same amplitude. As expected, $R_m^{(FC)}$ is reached when all the oscillators are simultaneously stimulated. The same is essentially true for T_m. For low amplitudes $A \leq 0.3$, the asymptotic shape observed in the fully coupled network is never reached, because the stimulation amplitudes are smaller or of the order of the minimal one required to elicit a burst in the fully coupled network.

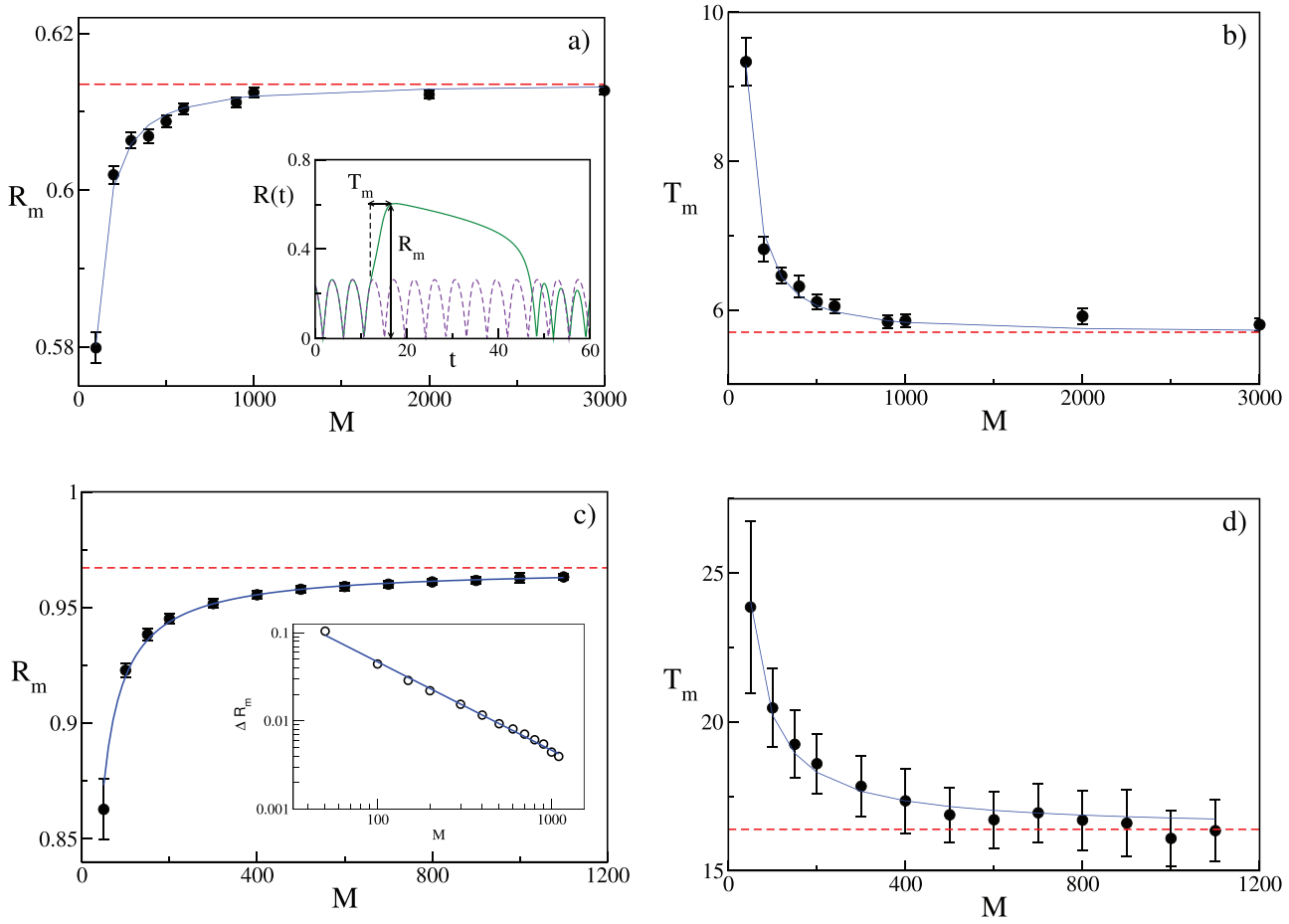

FIG. 3. BKM: System response to a global stimulation of amplitude $A = 0.4$: (a) maximum value of the order parameter R_m and (b) time T_m needed to reach it as a function of the degree M. KMI: System response to a global stimulation of amplitude $A = 6$: (c) maximum value of the order parameter R_m and (d) time T_m needed to reach it as a function of the degree M. In the inset in (a), a schematic picture explains how R_m and T_m are estimated in the case of the BKM, and the unperturbed (perturbed) evolution of $R(t)$ is displayed as a dashed violet (solid green) line. The red dashed lines represent, in all panels, the values obtained for the fully coupled network averaged over ten different initial conditions. The blue lines are nonlinear fitting to the data. For the maximum value of the order parameter, we employed the expression $R_m \simeq R_m^{(FC)} - a/M^\beta$ with $R_m^{(FC)} \simeq 0.6135$ ($\simeq$0.9672), where $a \simeq 15.86$ ($\simeq$4.75) and $\beta \simeq 1.34$ ($\simeq$1.00) for the BKM in (a) [KMI in (c)] and for the time needed to reach R_m $T_m \simeq T_m^{(FC)} + b/M^\beta$ with $T_m^{(FC)} \simeq 5.70$ ($\simeq$16.39), where $b \simeq 2638.60$ ($\simeq$385.23) and $\beta \simeq 1.43$ ($\simeq$1.00) for the BKM in (b) [KMI in (d)]. In the inset in (c), the data for $\Delta R_m = R_m^{(FC)} - R_m$ are reported vs M for the KMI in a log–log plot together with the corresponding power-law fitting a/M^β (blue solid line) with $a \simeq 4.75$ and $\beta = 1.00$. Data are averaged over 100 realizations, and the error bars correspond to the standard deviation of the mean. Other parameters are fixed as in Fig. 1, apart from $K = 4.0$ for the KMI.

All the analyses for the BKM have been so far performed for $N = 5000$. However, it is important, in at least one case, to evaluate the relevance of the finite size effects. Therefore, for a fixed degree $M = 200$ and perturbation amplitude $A = 0.5$, we examine the response of the network for different system sizes: $N = 1250$, 2500, 5000, and 10 000. The results of this analysis, reported in Fig. 5, show clear finite size effects for $N = 1250$ and $N = 2500$ whenever a percentage P of stimulated oscillators is chosen below 30%. As shown in the inset, the finite size effects become less and less relevant for increasing P; in particular, for small P-values ($P < 30\%$), the percentage of elicited bursts displays a power-law decay $\simeq N^{-\gamma}$ with an exponent γ strongly dependent on P. A linear extrapolation of the decay of this exponent $\gamma = \gamma(P)$ provides us with a critical value $P_c(A = 0.5) \simeq 28.7\%$ below which no burst can be elicited for sufficiently large system sizes. This represents an activation threshold to observe excitable properties in the system in the thermodynamic limit. Obviously, this threshold depends on the value of A, but this is a generic feature of the studied random network present for any perturbation amplitude $A \geq A_0$. On the other hand, above this threshold value, the finite size effects can be assumed to be negligible. Furthermore, since for $P = 30\%$, we have elicited bursts already in the 75%–77% of cases, we can affirm that the transition from no elicited bursts to a finite number of bursts should occur in an extremely narrow interval of P values in the thermodynamic

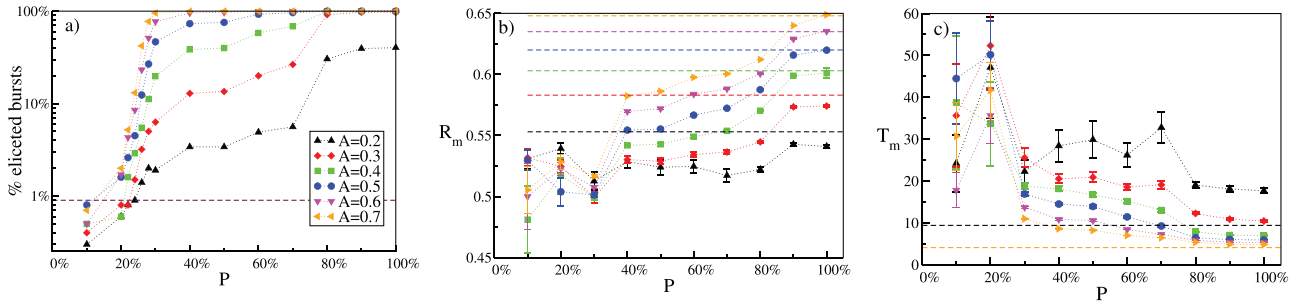

FIG. 4. BKM: System response to stimulations of various amplitudes applied to a different percentage P of oscillators for a fixed degree ($M = 200$). (a) Percentage of elicited bursts vs the percentage P of perturbed oscillators. Different curves represent simulations for different perturbation amplitudes A; the dashed horizontal line represents the percentage of spontaneous emissions. (b) Maximum value of the order parameter R_m, measured at the burst peak, vs P for different A values. (c) T_m is the time value for the system to reach the burst peak vs P for different A values. The dashed lines in panels (b) and (c) represent the values obtained from the simulations of the fully coupled networks for the corresponding stimulation amplitude A. The colors identify the different A values as reported in the legend in panel (a). In all panels, data are averaged over 1000 different realizations, and the error bars correspond to the standard deviation of the mean. See Fig. 1 for the parameters.

limit. The analysis of the nature of this transition, continuous or discontinuous, is left for future analysis.

Let us now examine the response of the system for a fixed perturbation amplitude for various degree values $M \in [100 : 900]$ corresponding to clustering coefficients in the range $c \in [2\% : 18\%]$ by varying the percentage P of stimulated oscillators. The corresponding results are reported in Fig. 6(a). The perturbation amplitude $A = 0.4$ has been chosen in order to be larger than the minimal excitability threshold A_0 already at $M = 100$. As a first remark, we observe that, below a stimulation threshold involving at least a percentage $P_m = 20\%$ of oscillators, almost no burst is elicited. Furthermore, the increase of M leads to a larger number of emitted bursts, once fixed the percentage of stimulated oscillators P. However, we observe 100% of elicited bursts only when at least a percentage $P_f = 80\%$ of oscillators is perturbed, irrespective of M, apart from $M = 100$ where a one to one correspondence between stimulation and burst occurrence is never achieved for this stimulation amplitude. Similarly, for $M \geq 200$, the quantities R_m and T_m, characterizing the burst, approach their fully coupled values for increasing P values that are reached whenever $P \geq P_f$ [see Figs. 6(b) and 6(c)].

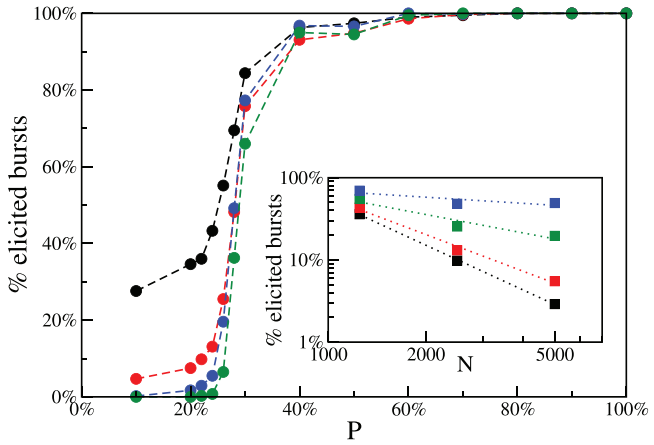

FIG. 5. BKM: Finite size effects for fixed degree $M = 200$ and amplitude of perturbation $A = 0.5$. Percentage of elicited bursts vs the percentage P of perturbed oscillators for various system sizes: $N = 1250$ (black circles), $N = 2500$ (red ones), $N = 5000$ (blue ones), and $N = 10\,000$ (green ones). The dashed lines are a guide for the eyes. The percentage of elicited bursts for different system sizes for various percentage P of stimulated oscillators is reported in the inset: namely, $P = 22\%$ (black squares), $P = 24\%$ (red squares), $P = 26\%$ (green squares), and $P = 28\%$ (blue squares). The dotted lines are power-law fitting to the data of the type $a + bN^{-\gamma}$, and the values of the estimated exponents are $\gamma \simeq 1.82$ ($P = 22\%$), $\gamma \simeq 1.49$ ($P = 24\%$), $\gamma \simeq 0.75$ ($P = 26\%$), and $\gamma \simeq 0.25$ ($P = 28\%$). The data are averaged over 1000 different realizations, apart from $N = 10\,000$, where only 200 realizations are considered. Other parameters as in Fig. 1.

In order to understand if the order of stimulation of the oscillators is relevant, we consider besides the standard protocol zero, employed in the rest of the article, also two other protocols (one and two), previously defined in Sec. II C. In particular, we analyze the excitable response of the network to these partial stimulations protocols for fixed degree $M = 200$ and fixed amplitude stimulation, namely, $A = 0.4$. The results of this analysis are displayed in Fig. 7. It is clear that the most effective protocol to induce excitable bursts is the protocol one, this because, by stimulating the oscillators with natural frequencies in correspondence with the peaks of the frequency distribution, favors the formation of synchronized clusters. On the other hand, the protocol two is the less effective one since the stimulations of oscillators with natural frequencies in proximity of only one peak result in an asymmetric recruitment of oscillators, which do not favor global synchronization. The protocol zero shares a similar problem by recruiting first the oscillators located in the minimum of the probability distribution function between the two peaks; indeed, the results are quite similar to protocol two apart from very large percentage P of stimulated oscillators (beyond 70%), where protocol zero performs better.

This is evident also by looking at the values obtained for R_m [shown in Fig. 7(b)], which are definitely smaller for protocols zero and two with respect to protocol one for the same percentage

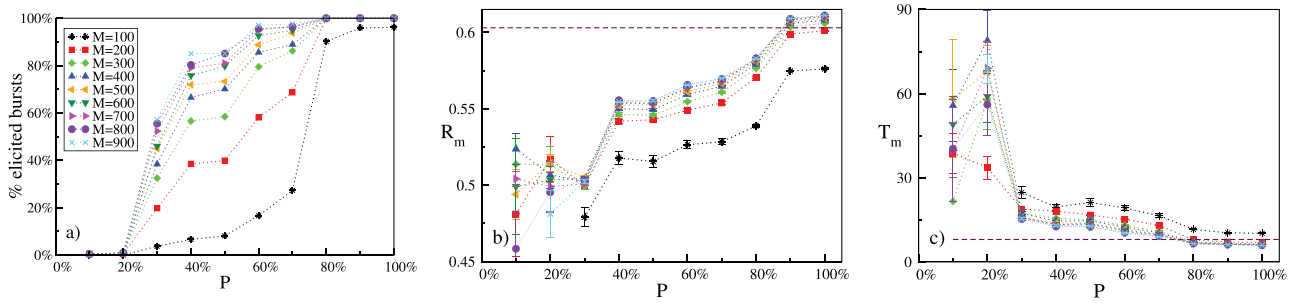

FIG. 6. BKM: System response to stimulations with fixed amplitude ($A = 0.4$) for different degrees M: percentage of elicited bursts (a), R_m (b), and T_m (c) vs the percentage P of perturbed oscillators. The black dashed lines represent the values for the fully coupled network $M = N$. Data are averaged over 1000 different realizations of the networks, and the error bars correspond to the standard deviation of the mean. See Fig. 1 for the other parameters.

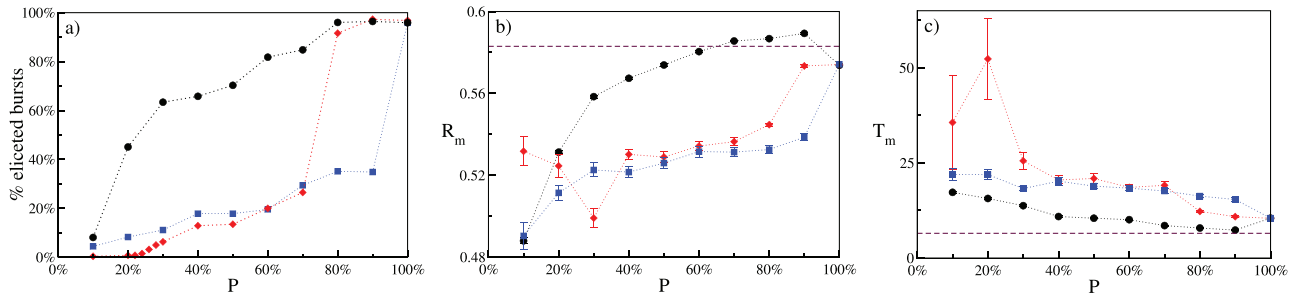

FIG. 7. BKM: Comparison among different perturbation protocols: protocol zero (red line with diamonds), protocol one (black line with circles), and protocol two (blue line with squares). Percentage of elicited bursts (a), R_m (b), and T_m (c) vs the percentage P of perturbed oscillators. The black dashed lines represent the values for the fully coupled network $M = N$. Data are averaged over 1000 realizations of the network, and the error bars correspond to the standard deviation of the mean. $A = 0.4$, $M = 200$; other parameters as in Fig. 1.

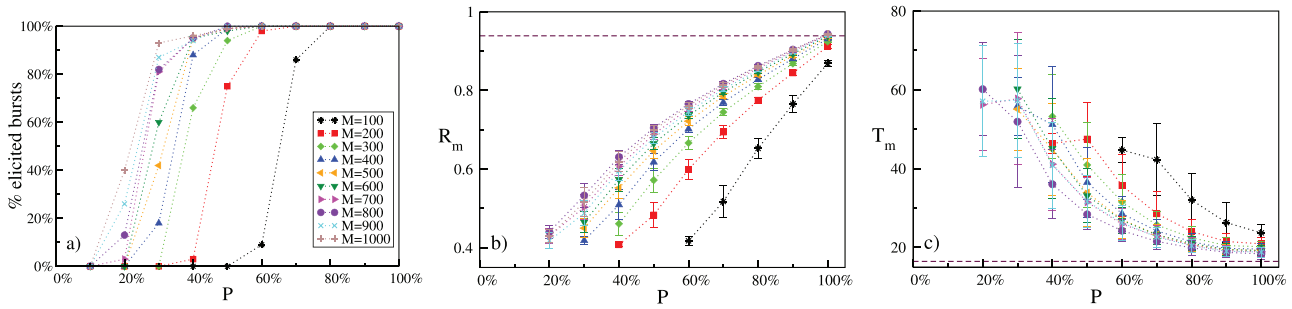

FIG. 8. KMI: System response to partial stimulation protocols with fixed amplitude ($A = 6$) for different degrees M: percentage of elicited bursts (a), R_m (b), and T_m (c) vs the percentage P of perturbed oscillators. The black dashed lines represent the fully coupled value. The data refer to an average over 100 different realizations of the network, and the error bars correspond to the standard deviation of the mean. See Fig. 1 for the other parameters.

P of stimulated oscillators. Indeed, the values of R_m for protocol one are already comparable to the fully coupled result for $P = 40\%$. Also, the activation of the oscillators involved in the burst is faster for protocol one than for the other two protocols, as shown in Fig. 7(c).

These results clearly indicate that a stimulation of oscillators guided by their natural frequency distribution is the optimal one to elicit more bursts involving more oscillators.

B. Kuramoto model with inertia

Finally, we present the results for the partial stimulation of KMI, where we investigate the response of the system for a fixed perturbation amplitude, while varying the degree M of the considered networks (see Fig. 8). We have chosen an amplitude $A = 6$ definitely larger than the minimal amplitude A_0 needed to ignite a burst for the KMI for any $M \geq 100$. At variance with the BKM case, the minimal percentage P_m of the stimulated oscillators, which is needed to observe a burst, as well as the critical percentage P_f required to observe 100% of elicited bursts, strongly depends on M. This is true at least for $M \leq 500$, corresponding to clustering coefficients $c \leq 0.25\%$, definitely smaller than those examined in the BKM case where $c \geq 2\%$. Indeed, for $M = 100$, one needs to stimulate 50% of the population to elicit a burst, while P_m decreases to 20% only for $M \geq 700$. Furthermore, we observe in this case that $P_f \simeq P_m + 30\%$; therefore, after the bursts' activation, a moderate increase in P leads to a one to one response to the stimulation. However, this is not connected with the achievement of the characteristics of the burst displayed in the fully coupled case. As shown in Figs. 8(b) and 8(c), the approach to the fully coupled values for R_m and T_m is quite gradual, and these are achieved only when essentially the whole network is stimulated. These effects are clearly due to the inertia present in the model that makes the single oscillators more resilient to stimulation.

V. CONCLUSIONS

Excitability is an important property of many living cells, such as neurons, whereby a large, rapid change in the membrane potential is generated in response to a very small stimulus. While its mechanisms are reasonably well understood at the level of the single elements, the origin of collective excitable phenomena in mesoscopic populations is less clear.

Of particular interest is the case of adaptive networks of globally coupled non-excitable units, in which the emergent macroscopic dynamics cannot be deduced in any way from the individual properties of the nodes. A key role here is played by the adaptive feedback, which allows for the coupling to slowly evolve as a function of the degree of synchrony of the system; thus, the network is permanently driven across a hysteretic phase transition.[14–16] The result is collective slow–fast dynamics, such as bursting and excitability via canard explosions, that arise even for small population sizes.[17]

In this work, we provided evidence of emergent collective excitability in highly diluted random networks of oscillators. This phenomenon has been studied for the Kuramoto model with and without inertia, considering different global and partial stimulation protocols and different levels of dilution.

In the case of global stimulation, we can observe excitable responses down to the dilution level of 1% for the BKM and 0.015% for the KMI by increasing the perturbation amplitude. Quite astonishingly, the KMI with a linear feedback can exhibit excitable responses down to a degree $M > 2$ for which the giant component emerges in the corresponding random network in the absence of adaptation.[32,33] This is in line with what was reported in Ref. 21, where it was shown that the hysteretic transition for the KMI persists down to a degree $M = 5$, but for a smaller network size, namely, $N = 5000$, where finite size fluctuations are larger than in the network of size $N = 20\,000$ here considered. As a general effect, the dilution reduces the level of synchronization R_m achieved during the collective burst and increases the time T_m needed to reach the peak of the burst for the same stimulation amplitude. In the limit $M \to N$, the fully coupled results are recovered and the finite size corrections due to the dilution vanish at the leading order as $\propto 1/M^{\beta}$, with $\beta \simeq 1.0 - 1.4$, by approaching the fully coupled limit.

For partial stimulation protocols, where only a certain percentage P of the oscillators is stimulated, the collective excitability emerges for $P \geq 20 - 30\%$ only. A detailed finite size analysis performed for the BKM at fixed dilution and perturbation amplitude suggests the existence of a phase transition from a nonexcitable to an excitable regime occurring for a finite percentage of stimulated oscillators P_c. The exact nature of the transition, continuous or discontinuous, is left to future analysis; however, it appears to be quite abrupt. Furthermore, for $P > P_c$, we observe that the excitable response of the system becomes more and more reliable, and finally, for $P \geq P_f$, elicited bursts are observable for any considered network realization. The threshold value P_f depends slightly on the level of dilution; however, it decreases strongly by increasing the amplitude A of the perturbation: namely, $P_f \propto 1/A^2$ for $A \geq 0.5$ and $M = 200$.

Another interesting aspect revealed by the analysis of the BKM is that the more effective way to induce collective excitable responses is to stimulate the oscillators accordingly to the distribution of their natural frequencies. In the case of bimodal distributions, this amounts to stimulate symmetrically the oscillators with frequencies in correspondence with the two peaks of the probability distribution function.

The inertia plays a fundamental role when partial stimulations are considered; indeed, at variance with the BKM case for a fixed stimulation amplitude, the minimal percentage P_m of oscillators to stimulate in order to observe at least one burst, as well as the threshold value P_f, strongly depends on M. Furthermore, an excitable response, analogous to that of a fully coupled network, is achieved only when the entire network is stimulated simultaneously, while for the BKM, this was already observable in most cases for $P \geq 80\%$.

Collective self-sustained behaviors characterized by irregular alternation between synchronized and desynchronized regimes have been previously reported for spiking neural networks in the presence of spike timing dependent plasticity (STDP).[34,35] The neurons considered in Ref. 35 were supra-threshold in a regime of tonic firing; therefore, they can be considered *de facto* as phase oscillators, even though in such a context, the emergent dynamics was not analyzed

in terms of collective excitability. In order to render our findings more general, it would be worth extending our analysis to plastic neural networks as well as to adaptive networks of phase oscillators with co-evolving pairwise couplings mimicking somehow Hebbian learning or STDP.[36,37]

Our work generalizes previous studies on globally coupled systems[14–17] to the case of highly diluted random networks and demonstrates remarkable robustness of macroscopic excitability induced by adaptive feedback. These results establish a bridge between the microscopic and mesoscopic dynamics, showing how sub-groups of oscillators can coherently combine themselves to produce a macroscopic burst, similarly to that of a single excitable cell. We expect that our work will inspire new research in the study of emergent phenomena in networks of interacting elements at the mesoscopic scale or even in more complex systems, such as networks composed of different kinds of functional units or networks of networks.

ACKNOWLEDGMENTS

A.T. received financial support from the Labex MME-DII (Grant No. ANR-11-LBX-0023-01) (together with MP) and from the ANR Project ERMUNDY (Grant No. ANR-18-CE37-0014), all part of the French program "Investissements d'Avenir." Part of this work has been developed during the visit of SO during 2021 to the Maison internationale de La Recherche, Neuville-sur-Oise, France supported by CY Advanced Studies, CY Cergy Paris Université, France.

AUTHOR DECLARATIONS

Conflict of Interest

The authors have no conflicts to disclose.

Author Contributions

Gabriele Paolini: Data curation (equal); Investigation (equal); Software (equal). **Marzena Ciszak:** Data curation (equal); Formal analysis (equal); Validation (equal); Writing – review & editing (equal). **Francesco Marino:** Conceptualization (equal); Writing – original draft (equal); Writing – review & editing (equal). **Simona Olmi:** Conceptualization (equal); Data curation (equal); Visualization (equal); Writing – review & editing (equal). **Alessandro Torcini:** Conceptualization (lead); Data curation (lead); Funding acquisition (lead); Project administration (lead); Writing – original draft (lead); Writing – review & editing (lead).

DATA AVAILABILITY

The data that support the findings of this study are available from the corresponding author upon reasonable request.

REFERENCES

[1] C. Kock, *Biophysics of Computation* (Oxford University Press, 1999).
[2] R. R. Aliev and A. V. Panfilov, Chaos, Solitons Fractals **7**, 293 (1996).
[3] J. L. Hindmarsh and R. M. Rose, Proc. R. Soc. London, Ser. B **221**, 87–102 (1984).
[4] D. Terman, J. Nonlinear Sci. **2**, 135 (1992).
[5] X.-J. Wang, Physica D **62**, 263 (1993).
[6] E. Mosekilde, B. Lading, S. Yanchuk, and Y. Maistrenko, BioSystems **63**, 3 (2001).
[7] J. M. González-Miranda, Chaos **13**, 845 (2003).
[8] G. Innocenti, A. Morelli, R. Genesio, and A. Torcini, Chaos **17**, 043128 (2007).
[9] S. Coombes and P. Bressloff, *Bursting: The Genesis of Rhythm in the Nervous System* (World Scientific Publishing Company, Singapore, 2005).
[10] Y. Kawamura, H. Nakao, and Y. Kuramoto, Phys. Rev. E **84**, 046211 (2011).
[11] E. Meron, Phys. Rep. **218**, 1 (1992).
[12] M. Ciszak, A. Montina, and F. T. Arecchi, Chaos **19**, 015104 (2009).
[13] A. Dolcemascolo, A. Miazek, R. Veltz, F. Marino, and S. Barland, Phys. Rev. E **101**, 052208 (2020).
[14] P. So and E. Barreto, Chaos **21**, 033127 (2011).
[15] P. S. Skardal, D. Taylor, and J. G. Restrepo, Physica D **267**, 27 (2014).
[16] M. Ciszak, F. Marino, A. Torcini, and S. Olmi, Phys. Rev. E **102**, 050201 (2020).
[17] M. Ciszak, S. Olmi, G. Innocenti, A. Torcini, and F. Marino, Chaos, Solitons Fractals **153**, 111592 (2021).
[18] D. Pazó and E. Montbrió, Phys. Rev. E **80**, 046215 (2009).
[19] E. A. Martens, E. Barreto, S. H. Strogatz, E. Ott, P. So, and T. M. Antonsen, Phys. Rev. E **79**, 026204 (2009).
[20] H.-A. Tanaka, A. J. Lichtenberg, and S. Oishi, Phys. Rev. Lett. **78**, 2104 (1997).
[21] S. Olmi, A. Navas, S. Boccaletti, and A. Torcini, Phys. Rev. E **90**, 042905 (2014).
[22] S. Olmi and A. Torcini, in *Control of Self-Organizing Nonlinear Systems* (Springer, 2016), pp. 25–45.
[23] E. Ott and T. M. Antonsen, Chaos **18**, 037113 (2008).
[24] J. Um, H. Hong, and H. Park, Phys. Rev. E **89**, 012810 (2014).
[25] G. Ódor and J. Kelling, Sci. Rep. **9**, 19621 (2019).
[26] S. Luccioli, S. Olmi, A. Politi, and A. Torcini, Phys. Rev. Lett. **109**, 138103 (2012).
[27] P. Erdos, A. Rényi *et al.*, Publ. Math. Inst. Hung. Acad. Sci. **5**, 17 (1960).
[28] E. Montbrió, D. Pazó, and A. Roxin, Phys. Rev. X **5**, 021028 (2015).
[29] J. A. Acebrón, L. L. Bonilla, C. J. Pérez Vicente, F. Ritort, and R. Spigler, Rev. Mod. Phys. **77**, 137 (2005).
[30] Y. Kuramoto, in *International Symposium on Mathematical Problems in Theoretical Physics* (Springer, 1975), pp. 420–422.
[31] E. M. Izhikevich, Int. J. Bifurc. Chaos **10**, 1171 (2000).
[32] M. E. Newman *et al.*, *Handbook of Graphs and Networks* (Wiley, 2003), Vol. 1, p. 35.
[33] M. Molloy and B. Reed, Random Struct. Algorithms **6**, 161 (1995).
[34] E. V. Lubenov and A. G. Siapas, Neuron **58**, 118 (2008).
[35] K. Mikkelsen, A. Imparato, and A. Torcini, Phys. Rev. Lett. **110**, 208101 (2013).
[36] T. Aoki and T. Aoyagi, Phys. Rev. Lett. **102**, 034101 (2009).
[37] R. Berner, S. Vock, E. Schöll, and S. Yanchuk, Phys. Rev. Lett. **126**, 028301 (2021).